



AIAA 2001-0243  
Flow Measurement Techniques  
for the Microfrontier

S.T. Wereley and L. Gui  
Purdue University  
West Lafayette, IN

**39th Aerospace Sciences Meeting & Exhibit**  
8–11 January 2001  
Reno, Nevada

## FLOW MEASUREMENT TECHNIQUES FOR THE MICROFRONTIER

**S. T. Wereley, L. Gui**

Mechanical Engineering, Purdue University  
West Lafayette, IN 47907-1288

**C. D. Meinhart**

Department of Mechanical and Environmental Engineering  
University of California, Santa Barbara, CA 93106

### **ABSTRACT**

The recent explosive increase in the use of fluidic micro-electromechanical systems (MEMS) has subsequently driven the development of fluidic measurement techniques capable of measuring velocities at length scales small enough to be of use in characterizing and optimizing these new devices. Recently, several techniques have demonstrated spatial resolutions smaller than 100  $\mu\text{m}$  but larger than 10  $\mu\text{m}$ . These techniques include X-Ray microimaging, molecular tagging velocimetry, and micro-laser Doppler velocimetry. However, measurements with spatial resolutions smaller than 10  $\mu\text{m}$  are necessary for making measurements in many MEMS applications. Only micro-PIV has demonstrated this high spatial resolution. By using a combination of advanced imaging and processing techniques that are described here, spatial resolutions on the order of single microns can be achieved.

### **INTRODUCTION**

There are several areas in science and engineering where it is important to determine the flow field at the micron scale. Industrial applications of microfabricated fluidic devices are present in the aerospace, computer, automotive, and biomedical industries. In the aerospace industry, for instance, micron-scale supersonic nozzles measuring approximately 35  $\mu\text{m}$  are being designed for JPL/NASA to be used as microthrusters on micro-satellites, and for AFOSR / DARPA as flow control devices for palm-size micro-aircraft (Bayt et al., 1997). In the computer industry, inkjet printers, which consist of an array of nozzles with exit orifices on the order of tens of microns in diameter, account for 65% of the computer printer market (Kamisuki, 1998). The biomedical industry is currently developing and using microfabricated fluidic devices for patient diagnosis, patient monitoring, and drug delivery. The I-STAT device (Affymetrix, Inc.) is the first microfabricated fluidic device that has been widely used in the medical community for blood analysis. Other examples of

microfluidic devices for biomedical research include micro-scale flow cytometers for cancer cell detection (Fuller, et al., 2000), micro-machined electrophoretic channels for DNA fractionation, and polymerase chain reaction (PCR) chambers for DNA amplification (Northrup et al., 1995). The details of the fluid motion through these small channels, coupled with nonlinear interactions between macromolecules, cells, and the surface-dominated physics of the channels create very complicated phenomena, which can be difficult to simulate numerically.

There has been a wide range of diagnostic techniques developed for experimental microfluidic research. Some of these techniques have been designed to obtain the highest spatial resolution and velocity resolution possible, while other techniques have been designed for application in non-ideal situations where optical access is limited (Lanzillo et al., 1996), or in the presence of highly scattering media (Chen et al., 1997).

Scalar Image Velocimetry (SIV) was developed by Dahm et al. (1992) for measurement of turbulent jets. A variation on SIV, Molecular Tagging Velocimetry (MTV) is a technique that has shown promise in microfluidics research. In this technique, flow-tracing molecules phosphoresce after being excited by a grid of UV light. Two CCD cameras image the phosphorescent grid lines with a short time delay between the two images. Local velocity vectors are estimated by correlating the grid lines between the two images (Koochesfahani et al. 1996). Paul et al. (1998) applied MTV to estimate velocity fields for pressure- and electrokinetically driven flows in 75  $\mu\text{m}$  diameter capillary tubes. Since MTV uses molecular tracers to follow the flow, it has several advantages at the micro scale over techniques such as PIV or LDV, which use discrete flow-tracing particles. However, molecular tracers have much higher diffusion coefficients that may significantly lower the spatial resolution and velocity resolution of the measurements.

The machine vision community developed a class of velocimetry algorithms, called optical-flow algorithms,

to determine the motion of rigid objects. The technique can be extended to fluid flows by assuming the effect of molecular diffusion is negligible, and requiring that the velocity field is sufficiently smooth. Since the velocity field is computed from temporal and spatial derivatives of the image field, the accuracy and reliability of the velocity measurements is strongly influenced by noise in the image field. This technique imposes a smoothness criterion on the velocity field, which effectively low-pass filters the data, and can lower the spatial resolution of the velocity measurements (Wildes et al., 1997). Lanzillotto et al. (1996) applied the optical-flow algorithms to infer velocity fields from 500–1000  $\mu\text{m}$  diameter micro-tubes by indirectly imaging 1-20  $\mu\text{m}$  diameter x-ray-scattering emulsion droplets in a liquid flow. High speed x-ray micro-imaging techniques were presented by Leu et al (1997). A synchrotron is used to generate high-intensity x-rays that scatter off the emulsion droplets onto a phosphorous screen. A CCD camera imaging the phosphorous screen detects variations in the scattered x-ray field. The primary advantage of x-ray imaging technique is that one can obtain structural information about the flow field, without having optical access. Hitt et al. (1996) applied the optical flow algorithm to *in vivo* blood flow in microvascular networks, with diameters  $\sim 100 \mu\text{m}$ . The algorithm spectrally decomposes sub-images into discrete spatial frequencies, by correlating the different spatial frequencies to obtain to obtain flow field information. The advantage of this technique is that it does not require discrete particle images to obtain reliable velocity information. Hitt et al. (1995) obtained *in vivo* images of blood cells flowing through a microvascular network using a 20x water immersion lens with a spatial resolution on the order of 20  $\mu\text{m}$  in all directions.

Laser Doppler Velocimetry (LDV) has been a standard optical measurement technique in fluid mechanics over the past 25 years. In the case of a dual-beam LDV system, the volume of the intersection of the two laser beams defines the measurement volume. Traditionally, the measurement volumes of standard LDV systems have characteristic dimensions on the order of a few millimeters. Compton and Eaton (1996) used short focal length optics to obtain a measurement volume of 35  $\mu\text{m} \times 66 \mu\text{m}$ . Using very short focal length lenses, Tieu et al. (1995) built a dual-beam solid-state LDA system that has a measurement volume of approximately 5  $\mu\text{m} \times 10 \mu\text{m}$ . Their micro LDV system was used to measure the flow through a 175  $\mu\text{m}$  thick channel, producing time-averaged measurements that compare well to the expected parabolic velocity profile, except within 18  $\mu\text{m}$  of the wall. Advancements in microfabrication

technology are expected to facilitate the development of new generations of self-contained solid-state LDV systems with micron-scale probe volumes. These systems will likely serve an important role in diagnosis and monitoring of microfluidic systems (Modarress et al. 1998, 2000). However, the size of the probe volume significantly limits the number of fringes that it can contain which subsequently limits the accuracy of the velocity measurements.

Optical Doppler Tomography (ODT) has been developed to measure micron-scale flows embedded in a highly scattering medium. In the medical community, the ability to measure *in vivo* blood flow under the skin allows clinicians to determine the location and depth of burns (Chen et al., 1997). ODT combines single-beam Doppler velocimetry, with heterodyne mixing from a low-coherence Michelson interferometer. The lateral spatial resolution of the probe volume is determined by the diffraction spot size. The Michelson interferometer is used to limit the effective longitudinal length of the measurement volume to that of the coherence length of the laser. The ODT system developed by Chen et al. (1997) has a lateral and longitudinal spatial resolution of 5  $\mu\text{m}$  and 15  $\mu\text{m}$ , respectively. The system was applied to measure flow through a 580  $\mu\text{m}$  diameter conduit.

Particle Image Velocimetry (PIV) can be used to obtain high spatial resolution 2-D velocity fields. Santiago, et al. (1998) developed a micro-PIV system capable of measuring slow flows—velocities on the order of tens of microns per second—with a spatial resolution of 6.9 $\times$ 6.9 $\times$ 1.5  $\mu\text{m}$ . The system used an epi-fluorescent microscope and an intensified CCD camera to record 300 nm diameter polystyrene flow-tracing particles. The particles are illuminated using a continuous Hg-arc lamp. The continuous Hg-arc lamp is chosen for situations that require low levels of illumination light (e.g. flows containing living biological specimens) and where the velocity is sufficiently small so that the particle motion can be frozen by the CCD camera's electronic shutter.

Later applications of the micro-PIV technique moved steadily toward faster flows more typical of aerospace applications. The Hg-arc lamp was replaced with a New Wave two-headed Nd:YAG laser that allowed cross correlation analysis of singly-exposed image pairs acquired with sub-microsecond time steps between images. At macroscopic length scales this short time step would allow analysis of supersonic flows. However, because of the high magnification, the maximum velocity measurable with this time step is on the order of meters per second. Meinhart, et al., (1999)

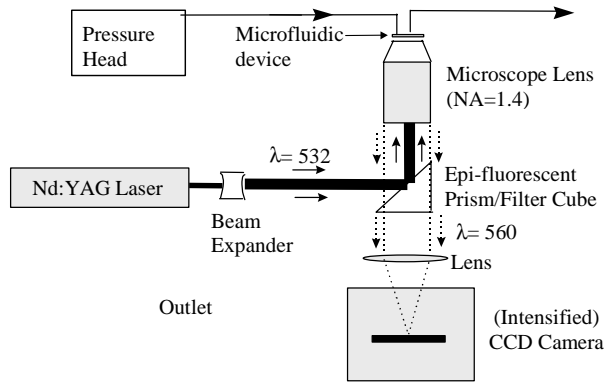


**Fig. 1.** Diagram of typical micro-PIV system.

applied micro PIV to measure the flow field in a  $30 \mu\text{m}$  high  $\times$   $300 \mu\text{m}$  wide rectangular channel, with a flow rate of  $50 \mu\text{l/hr}$ , equivalent to a centerline velocity of  $10 \text{ mm/s}$  or three orders of magnitude than the initial effort a year before. The experimental apparatus, shown in Figure 1, images the flow with a  $60\times$ ,  $\text{NA}=1.4$ , oil-immersion lens. The  $200 \text{ nm}$  diameter polystyrene flow-tracing particles were chosen small enough so that they faithfully followed the flow and were 150 times smaller than the smallest channel dimension. A subsequent investigation by Meinhart and Zhang (2000) of the flow inside a microfabricated ink jet printer head yielded the highest speed measurements made with micro-PIV. Using a slightly lower magnification ( $40\times$ ) and consequently lower spatial resolution, measurements of velocities as high as  $8 \text{ m/s}$  were made. In the following the authors will give an overview of micro-PIV techniques, and provide several application examples.

## OVERVIEW OF MICRO-PIV

### Fundamental physics of micro-PIV

Three fundamental problems differentiate micro-PIV from conventional macroscopic PIV: the particles become small compared to the wavelength of the illuminating light; the particles become small enough that the effects of Brownian motion must be addressed; and the illumination source is typically not a light sheet but rather an illuminated volume of the flow.

**Particles small compared to  $\lambda$**  Flow-tracing particles must also be large enough to scatter sufficient light so that their images can be recorded. In the Rayleigh scattering regime, where the particle diameter  $d$  is much smaller than the wavelength of light,  $d \ll \lambda$ , the amount of light scattered by a particle varies as  $d^6$  (Born and Wolf, 1997). Since the diameter of the flow-tracing particles must be small enough that the particles not disturb the flow being measured, they can frequently be on the order of  $50 \text{ nm} - 100 \text{ nm}$ . Their diameters are

then  $1/10$  to  $1/5$  the wavelength of green light,  $\lambda = 532 \text{ nm}$ , and are therefore approaching the Rayleigh scattering criteria. This places significant constraints on the image recording optics, making it extremely difficult to record particle images.

One solution to the imaging problem is to use epi-fluorescence imaging to record inelastically-scattered light from fluorescently-labeled particles through an optical filter, which removes the background light. This technique was used successfully in liquid flows to record images of  $200 - 300 \text{ nm}$  diameter fluorescent particles. While fluorescently-labeled particles are well suited for micro-PIV studies in liquid flows, they are not applicable to high-speed air flows for several reasons. First, commercially available fluorescently-labeled particles are available only in aqueous solutions. In principle, the particle-laden solutions can be dried, and the particles emitted into an air stream. Unfortunately, we have not been able to dry particles without significant particle clumping. Furthermore, the emission decay time of many fluorescent molecules is on the order of several nanoseconds, which may cause streaking of the particle images for high-speed flows. Presently, seeding gas flows remains a significant problem in micro-PIV.

**Effects of Brownian Motion** When the seed particle size becomes small, the effect of a single collision with an energetic fluid molecule becomes increasingly important. Santiago, et al. (1998) considered the effect of Brownian motion on the accuracy of PIV measurements. Assuming the seed particles having an Einstein diffusion coefficient  $D$  are in a steady, uniform flow of velocity  $u$  for a time duration  $\Delta t$ , one can estimate the relative error due to Brownian motion  $\epsilon_B$  by

$$\epsilon = \frac{1}{u} \sqrt{\frac{2D}{\Delta t}} \quad (1)$$

Santiago (1998) considered a flow with a characteristic velocity of  $u \sim 50 \mu\text{m s}^{-1}$ , diffusion coefficient of the  $300 \text{ nm}$  particles is  $D \sim 0.69 \mu\text{m}^2 \text{ s}^{-1}$ , and time between images is  $\Delta t = 68.5 \text{ ms}$ , yielding a relative error of approximately 9% for a single particle. Since this error results from random Brownian motion of water molecules bombarding the flow-tracing particles, it is an unbiased error that can be reduced by averaging over groups of particles. Because each PIV interrogation region contains a small group of particles and the resulting cross-correlation function is ensemble-averaged over several realizations, the error in the resulting velocity vector is substantially reduced. Assuming that each particle in the ensemble of

interrogation regions contributes equally to the average velocity vector and that they are statistically independent, the uncertainty due to Brownian motion of the ensemble-averaged velocity is approximately  $\epsilon_B / \sqrt{N}$ , where  $N$  is the total number of particles in the average.

Equation 1 demonstrates that the effect of Brownian motion is relatively less important for faster flows however for a given measurement, when  $u$  increases,  $\Delta t$  will generally be decreased. Equation 1 also demonstrates that when all conditions but the  $\Delta t$  are fixed, going to larger  $\Delta t$  will decrease the relative error introduced by Brownian motion. However, longer  $\Delta t$  will decrease the accuracy of the results because the PIV measurements are based on a first order accurate approximation to the velocity. Using a second order accurate technique (called CDI and presented below) allows for longer  $\Delta t$  to be used without increasing this error.

**Volume Illumination of Flow** The third significant difference between micro-PIV and macroscopic PIV is that due to lack of optical access, a light sheet can typically not be used to illuminate the flow. The flow must be volume illuminated, leaving two choices for how to visualize the seed particles—with an optical system whose depth of focus exceeds the depth of the flow being measured or with an optical system whose depth of focus is small compared to that of the flow. Both of these techniques have been used in various implementations of micro-PIV. Cummings (2001) uses a large depth of focus to explore electrokinetic and pressure driven flows. The advantage of the large depth of focus optical system is that all particles in the field of view of the optical system are well focused. The disadvantage of this scheme is that all depth information is lost and the resulting velocity fields are completely depth averaged. Cummings (2001) addresses this problem with advanced processing techniques that will not be covered here.

The second choice of optical systems was to choose one whose depth of focus is smaller than that of the flow domain. Then the optical system will focus those particles that are within the depth of focus of the imaging system and the remaining particles will be unfocused and contribute to the background noise level. Since the optical system is being used to define thickness of the measurement domain, it is important to characterize exactly how thick the depth of focus, or more appropriately, the depth of correlation, is. Meinhart, et al., (2000a) have considered this question in detail and derived the equation

$$\delta z_m = \frac{3n\lambda_0}{NA^2} + \frac{2.16d_p}{\tan\theta} + d_p \quad (2)$$

where  $\delta z_m$  is the measurement thickness,  $\lambda_0$  is the collected light wavelength,  $n$  is the refractive index of medium the lens is immersed in,  $NA$  is the numerical aperture of the optical system,  $\theta$  is the collection angle of the optical system, and  $d_p$  is the diameter of the seed particles. This equation demonstrates that the depth of correlation is a complicated function of experimental parameters that must be carefully evaluated for every experimental situation, even if only a minor variable such as the wavelength of illumination is changed. The depth of correlation can range from 1.8  $\mu\text{m}$  for a 60x oil immersion lens imaging 200 nm particles to 3.4  $\mu\text{m}$  for a 60x oil immersion lens imaging 1  $\mu\text{m}$  particles to 8.6  $\mu\text{m}$  for a 40x air immersion lens imaging 1 mm particles. Olsen and Adrian (2001) have developed a similar expression from a different approach which shows that Brownian motion will affect the depth of correlation.

One important implication of volume illumination that affects both large and small depth of focus imaging systems is that all particles in the illuminated volume will contribute to the recorded image. This implies that the particle concentrations will have to be minimized for deep flows and leads to the use of low image density images as described below.

### **Special processing methods for micro-PIV recordings**

When evaluating digital PIV recordings with conventional correlation-based algorithms or image-pattern tracking algorithms, a sufficient number of particle images are required in the interrogation window or the tracked image pattern to ensure reliable and accurate measurement results. However, in many cases, especially in micro-PIV measurements, the particle image density in the PIV recordings is usually not high enough (e.g. Fig. 2a). These PIV recordings are called low image density (LID) recordings and are usually evaluated with particle-tracking algorithms. When using particle-tracking algorithms, the velocity vector is determined with only one particle, and hence the reliability and accuracy are of the technique are limited. In addition, interpolation procedures are usually necessary to obtain velocity vectors on the desired regular grid points from the random distributed particle-tracking results (e.g. Fig. 3a), and therefore, additional uncertainties are added to the final results. Fortunately, some special processing methods can be used to evaluate the micro-PIV recordings, so that the errors resulting from the low image density can be avoided. In

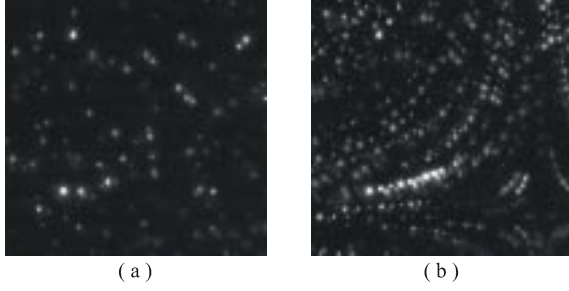


**Fig.2:** Example of image overlapping: (a) one of the LID-PIV recordings; (b) result of overlapping 9 LID-PIV recordings. Image size: 256×256 pixels

this section two methods are introduced to improve measurement accuracy of micro-PIV by using a digital image processing technique and by improving the evaluation algorithm, respectively.

**Overlapping of LID-PIV recordings** In early days of PIV, multiple exposure imaging techniques were used to increase the particle image numbers in PIV recordings. Similar to multiply exposing a single frame, high-image-density (HID) PIV recordings can be generated by computationally overlapping a number of LID-PIV recordings with

$$g_o(x, y) = \max\{g_k(x, y), k = 1, 2, 3, \dots, N\} \quad (3)$$

Wherein  $g_k(x, y)$  is the gray value distributions of the LID-PIV recordings with a total number  $N$ , and  $g_o(x, y)$  is the overlapped recording. Note that in Equation (3) the particle images are positive, i.e. with bright particles and dark background; otherwise the images should be inverted. An example of the image overlapping can be seen in Fig. 2b for overlapping 9 LID-PIV recordings. The size of the PIV recordings in Fig.2 is 256×256 pixels, and the corresponding measurement area is  $2.5 \times 2.5 \text{ mm}^2$ . The effect of the image overlapping is

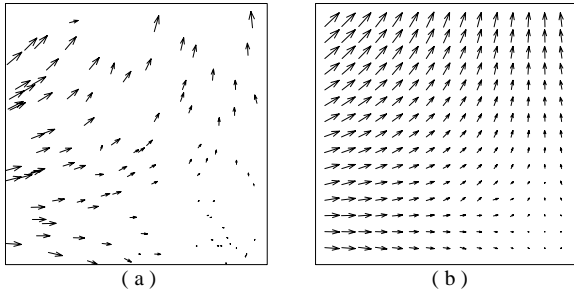


**Fig. 3:** Effect of image overlapping: (a) results for a single LID-PIV recording pair with a particle-tracking algorithm; (b) results for the overlapped PIV recording pair with a correlation-based algorithm

shown in Fig. 3. Fig. 3a is the evaluation results for one of the LID-PIV recording pairs with a particle-tracking algorithm (Gui et al. 1997), and Fig. 3b is the results for the overlapped PIV recording pair (out of 9 LID-PIV recording pairs) with a correlation-based algorithm. The results in Fig. 3b are more reliable, more dense, and more regularly spaced than those in Fig. 3a.

The image overlapping method is based on the fact that flows in microdomains typically have very low Reynolds numbers, so that the flow can be considered as laminar and steady in the data acquisition period. Note that this method cannot be extended to measurements of turbulent or unsteady flows, and it may not work very well when overlapping HID-PIV recordings or too many LID-PIV recordings because with large numbers of particle images, interference between particle images will occur.

**Ensemble correlation method** For correlation-based PIV evaluation algorithms the correlation function at a certain interrogation spot is usually represented as

$$\Phi_k(m, n) = \sum_{j=1}^q \sum_{i=1}^p f_k(i, j) \cdot g_k(i + m, j + n) \quad (4)$$

where  $f_k(i, j)$  and  $g_k(i, j)$  are the gray value distributions of the first and second exposure, respectively, in the  $k^{\text{th}}$  PIV recording pair at certain interrogation spot of size of  $p \times q$  pixels. The correlation function for a singly-exposed PIV image pair has a peak at the position of the particle image displacement in the interrogation spot (or window), which should be the highest among all the peaks of  $\Phi_k$ . The sub peaks, which result from noise or mismatch of particle images, are usually obviously lower than the main peak, i.e. the peak of the particle image displacement. However, when the interrogation window does not contain enough particle images or the noise level is too high, the main peak will become weak and may be lower than some of the “sub” peaks, and as such, an erroneous velocity vector is generated. In the laminar and steady flows measured by the micro-PIV system, the velocity field is independent of the measurement time. That means the main peak of  $\Phi_k(m, n)$  is always at the same position for PIV recording pairs taken at different times while the sub peaks appear with random intensities and positions in different recording pairs. Therefore, when averaging  $\Phi_k$  for enough number of PIV recording pairs ( $N$ ), the main peak will be kept at the position of the particle image displacement with the same intensity level, but the sub peaks will disappear. The averaged (or ensemble) correlation function is given as

$$\Phi_{ens}(m, n) = \frac{1}{N} \sum_{k=1}^N \Phi_k(m, n) \quad (5)$$

Just as with the image overlapping method detailed above, the ensemble correlation requires a steady flow. However, in contrast with the image overlapping method, the technique is not limited to LID recordings or to a small number of recordings. The concept of averaging correlation functions can also be applied to other evaluation algorithms such as correlation tracking and the MQD method. This method was first proposed and demonstrated by Meinhart, et al. (2000b).

The ensemble correlation function technique is demonstrated for 101 LID-PIV recording pairs ( $\Phi_{ens}$ ) is given in Fig. 3 in comparison to the evaluation function for one of the single recording pair ( $\Phi_k$ ). These PIV recording pairs are chosen from the flow measurement in a microfluidic biochip for impedance spectroscopy of biological species (Gomez et al. 2000). With the conventional evaluation function in Fig. 4a, the main peak cannot easily be identified among the sub peaks, so that the evaluation result is neither reliable nor accurate. However, the ensemble correlation function in Fig. 4b shows a very clear peak at the particle image displacement, and the sub peaks can hardly be recognized.

The effect of the ensemble correlation technique on the resulting velocity field is demonstrated in Fig. 5 with the PIV measurement of flow in the microfluidic biochip. All the evaluation errors resulting from the low image density and strong background noise (see Fig. 5a) are avoided by using the ensemble correlation method based on 101 PIV recording pairs (Fig. 5b). One important note here is that since the bad vectors in Fig. 5a all occur at the lower left corner of the flow domain, removal of these bad vectors and subsequent replacement by interpolated vectors will necessarily generate results that bear little resemblance to the true velocity field in the device.

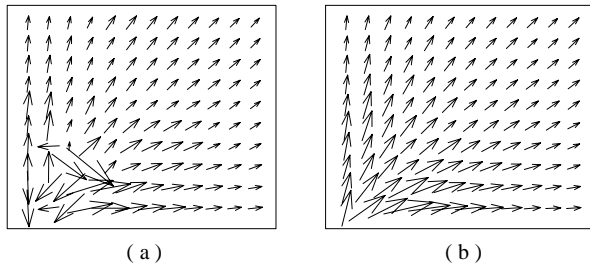


**Fig. 4:** Comparison of the evaluation function of a single PIV recording pair (a) with the average of 101 evaluation functions (b)

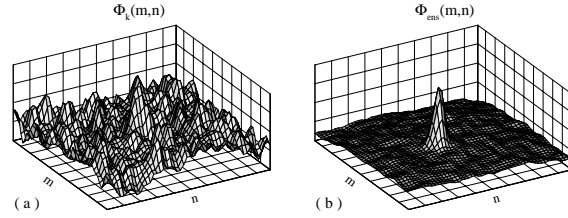


**Fig. 5:** Effect of ensemble correlation: (a) results with conventional correlation for one of the PIV recording pairs; (b) results with ensemble correlation for 101 PIV recording pairs.

### **Advanced processing methods for micro-PIV recordings**

For further improving the reliability and accuracy of micro-PIV measurements a number of evaluation techniques, which also work well for standard PIV systems, are applied. It is known that the measurement uncertainty of PIV data includes both bias error and precision error. One of the most effective methods for reducing the bias error of PIV measurements in complex flows is the Central Difference Interrogation (CDI) method. While for reducing the precision (or random) error, image correction methods are suggested. The CDI method and one of the image correction methods are introduced below.

**Central Difference Interrogation (CDI)** Currently, the adaptive window offset is widely used with the FFT-based correlation algorithm for reducing the evaluation error and with the image pattern tracking algorithms for increasing the spatial resolution. The adaptive window offset method, as typically implemented, can be referred to as Forward Difference Interrogation (FDI), because the second interrogation window is shifted in the forward direction of the flow an amount equal to the mean displacement of the particle images initially in the first window. Although the FDI method leads to significant improvements in the evaluation quality of PIV recordings in many cases, there are still some potentially detrimental bias errors that cannot be avoided with FDI, for instance, the position deviation in flows with large velocity gradients and direction deviation in flows with large curvature. The CDI method was initially introduced by Wereley, et al., (1998) and further developed and explored by Wereley and Meinhart (2000a,b), to avoid the shortcoming of FDI and increase the accuracy of the PIV measurement. When using CDI, the first and second interrogation window are shifted backwards and forwards,

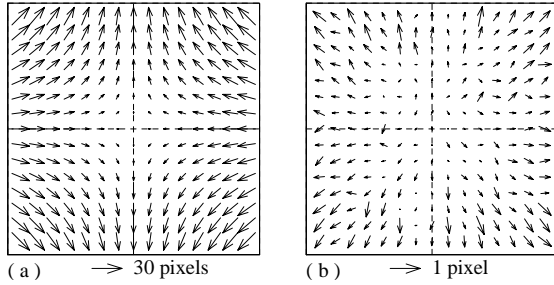


**Fig. 6:** Simulation of the four-roll-mill test: (a) desired flow pattern; (b) evaluation errors with FDI

respectively, with half of the expected particle image displacement. As with many adaptive window shifting techniques, this technique requires some iteration to achieve optimum results.

In order to demonstrate the advantage of CDI over the FDI, a typical curvature flow, i.e. the flow in a four-roll-mill, is used here as an example. According to the experimental condition, PIV recording pairs are simulated with the desired flow field shown in Fig. 6a. The maximal particle image displacement in the PIV recording pair of size of  $1024 \times 1024$  pixels is about 30 pixels. The corresponding measurement area and the maximal velocity are  $10 \times 10 \text{ mm}^2$  and  $0.04 \text{ mm/s}$ , respectively. When combining the FFT-based correlation algorithm with FDI, evaluation errors of a pair of the simulated recordings are determined by subtracting the desired flow field from the evaluation results and given in Fig. 6b. The evaluation errors in Fig. 6b seem to be dominated by bias errors that depend on the radius, i.e. the distance between the vector location and the flow field center.

In this test the bias errors are determined by averaging 500 individual error maps as shown in Fig. 6b, and a distribution of RMS values of the random errors is further computed. Dependences of the bias and random errors on the location (radius) are determined and shown in Fig. 7a and 7b for the FDI and CDI, respectively. The total error is defined as the root-sum-square (RSS) of the bias and random error. It is shown in Fig. 7 that the evaluation error of FDI is dominated by the bias error, when the radius is greater than 200 pixels. And when CDI is used, the bias error is so small that it can be neglected. The random error does not depend on the location, and replacing FDI with CDI does not change the random error level.

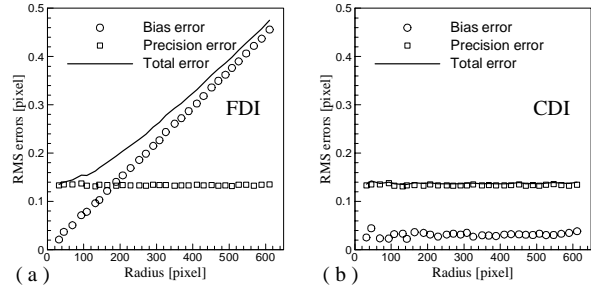


**Fig. 7:** Dependences of evaluation errors on the location (radius) of the evaluation with FDI (a) and CDI (b) for the four-roll-mill test

**Image correction technique** In the above example the bias error of the four-roll-mill test is minimized by using the CDI method. In order to further reduce the measurement uncertainty, i.e. the total error, the random errors must also be reduced. In the four-roll-mill test case, even when the flow is ideally seeded and the PIV recordings are made without any noise, evaluation errors may result from the deformation of the measured flow. To account for the deformation of the PIV image pattern, image correction techniques are developed. The idea of image correction was presented by Huang, et al., (1997), and the similar ideas were also applied by others. However, since the image correction was a complex and time-consuming procedure, it has not been widely used. In order to accelerate the evaluation, the authors modified the image correction method as follows: According to the previous evaluations, the particle image displacements at the four corners of the interrogation window are determined and used to correct the image patterns in the interrogation area for both exposures of the PIV recording pair, so that the image patterns have a good match at the particle image displacement. Combining the modified image correction with the FFT-based correlation algorithm, the

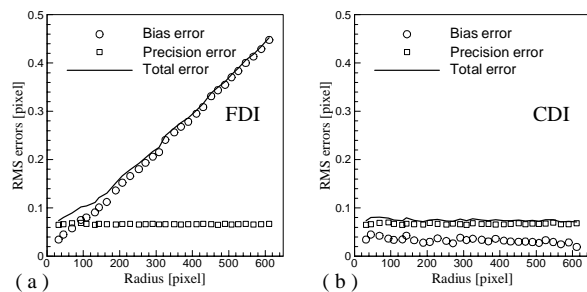


**Fig. 8:** Dependences of evaluation errors on the location of the evaluation with FDI (a) and CDI (b) by using image correction

evaluation can be run at a very high speed. The effect of the image correction is presented in Fig. 8. When combining the CDI with the image correction, the total error is effectively minimized.

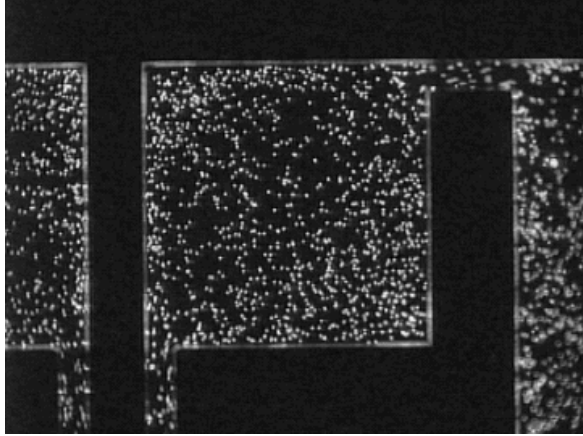


**Fig. 9:** Digital image of the seeded flow in the cavities and channels of the biochip (360×270 pixels, 542×406  $\mu\text{m}^2$ )

### MICRO-PIV EXAMPLES

#### Flow in Microfluidic Biochip

Microfluidic biochips are microfabricated devices that are used for delivery, processing and analysis of biological species (molecules, cells, etc.). Gomez et al. (2000) successfully used micro-PIV to measure the flow in a microfluidic biochip for impedance spectroscopy of biological species. The biochip used for the PIV experiment is fabricated in a silicon wafer with a thickness of 450  $\mu\text{m}$ . It has a series of rectangular cavities connected by channels with a depth of 12 $\mu\text{m}$ . The surface of the chip is covered with a piece of glass of about 0.2 mm thick, so that the images of seeded flows can be taken from the top. During the experiment, water-based suspensions of fluorescein-labeled latex beads with a mean diameter of 1.88  $\mu\text{m}$  were injected into the biochip. The flow is illuminated with a constant intensity mercury lamp. Images are captured with a CCD camera through an epi-fluorescence microscope and recorded at a video rate (30Hz).

One of the PIV images covering an area of 542×406  $\mu\text{m}^2$  on the chip with a digital resolution of 360×270 pixels is shown in Fig. 9. The flow in a rectangular cavity of the biochip is determined by evaluating more than 100 micro-PIV recording pairs with the ensemble correlation method, CDI and the

image correction technique, and the results are given in Fig. 10. An interrogation window of 8×8 pixels is chosen for the PIV image evaluation, so that the corresponding spatial resolution is about 12×12  $\mu\text{m}^2$ . The measured velocities in the cavity range from about 100  $\mu\text{m/s}$  to 1600  $\mu\text{m/s}$ .

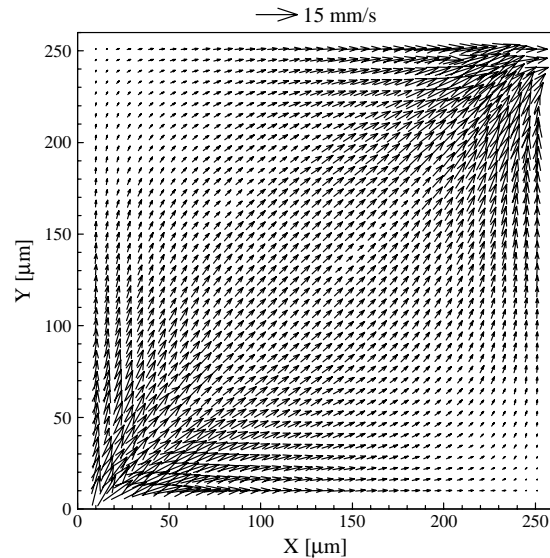


**Fig. 10:** PIV measurement results in a rectangular cavity of the biochip with a spatial resolution of 12×12  $\mu\text{m}^2$

### FUTURE DIRECTIONS – CONCLUSION

Currently, the maximum spatial resolution of the micro-PIV technique stands at approximately 1  $\mu\text{m}$ . By using smaller seed particles that fluoresce at shorter wavelengths, this limit could be reduced by a factor of 2 to 4. This lower limit of approximately 250 nm should be regarded as a hard limit for correlation-based PIV using visual wavelength light. Higher spatial resolutions could still be obtained by adding a particle tracking step after the correlation-based PIV. Spatial resolutions an order of magnitude smaller could then reasonably be reached.

The largest problem with respect to conducting micro-PIV experiments in gas flows is seeding. With adequate seeding, all of the results presented here could be extended to gas flows.

### ACKNOWLEDGEMENT

The biochip experiments were conducted by Raphael Gomez and Heather Apple, students at Purdue University. Professor Rashid Bashir made one of the

biochips available for testing. The simulated four roll mill data was inspired by Professor Gary Leal and Derek Tretheway at the University of California, Santa Barbara. This work was supported by the Indiana 21<sup>st</sup> Century Research and Technology Fund, the School of Mechanical Engineering at Purdue University, and 3M Corp.

## REFERENCES

- Bayt RL, Ayon AA, Breuer KS** 1997, A performance evaluation of MEMS-based micronozzles. *AIAA Paper 97-3169, 33<sup>rd</sup> AIAA/ASME/SAE/ASEE Joint Propulsion Conference & Exhibit*, July 7-9, Seattle, WA
- Born M, Wolf E** 1997. Principles of Optics. *Pergamon Press*.
- Chen Z, Milner TE, Dave D, Nelson JS** 1997, Optical Doppler tomographic imaging of fluid flow velocity in highly scattering media. *Optics Letters*, Vol. 22: pp. 64-66
- Compton DA, Eaton JK** 1996, A high-resolution laser Doppler anemometer for three-dimensional turbulent boundary layers. *Exp. Fluids* 22: 111-117
- Cummings EB** 2001, An image processing and optimal nonlinear filtering technique for PIV of microflows, *Exp. Fluids*, in press
- Dahm WJA, Su LK, Southerland KB** 1992, A scalar imaging velocimetry technique for fully resolved four-dimensional vector velocity field measurements in turbulent flows. *Physics of Fluids A (Fluid Dynamics)*, Vol. 4, No. 10, pp. 2191 – 2206
- Fuller CK, Hamilton J, Ackler H, Krulevitch P, Boser B, Eldredge A, Becker F, Yang J, Gascoyne P** 2000, Microfabricated multi-frequency particle impedance characterization system. *Proc.  $\mu$ TAS2000*, Enschede, The Netherlands, May
- Gui L, Merzkirch W, Shu JZ** 1997, Evaluation of low image density PIV recordings with the MQD method and application to the flow in a liquid bridge. *Journal of Flow Visualization and Image Processing*, Vol. 4, No. 4, pp. 333-343
- Hitt DL, Lowe ML, Tincher JR, Watters JM** 1996, A new method for blood velocimetry in the microcirculation. *Microcirculation*, Vol. 3 No. 3, pp. 259-263
- Hitt DL, Lowe ML, Newcomer R** 1995, Application of optical flow techniques to flow velocimetry. *Phys. Fluids* 7, No. 1, pp. 6–8
- Huang H, Dabiri D, Gharib M** 1997, On error of digital particle image velocimetry, *Meas. Sci. Technol.*, Vol. 8, pp. 1427-40.
- Kamisuki S, Hagata T, Tezuka C, Nose Y, Fujii M, Atobe M** 1998, A low power, small, electrostatically-driven commercial inkjet head. *Proceedings of MEMS'98*
- Koochesfahani MM, Cohn RK, Gendrich CP, Nocera DG** 1996, Molecular tagging diagnostics for the study of kinematics and mixing in liquid phase flows. *Proceedings in the Eighth International Symposium on Applications of Laser Techniques to Fluid Mechanics*, Lisbon, Portugal, July 8-11
- Lanzillotto AM, Leu TS, Amabile M, Wildes R, Dunsmuir J** 1996, Applications of x-ray micro-imaging, visualization and motion analysis techniques to fluidic microsystems. *Proceedings from Solid-state sensors and actuators workshop*, June 13-16, Hilton Head, SC
- Leu TS, Lanzillotto AM, Amabile M, Wildes R** 1997, Analysis of fluidic and mechanical motions in MEMS by using high speed x-ray micro-imaging techniques. *1997 International Conference on Solid-State Sensors and Actuators*, June 16-19, Chicago
- Meinhart CD, Wereley ST, Santiago JG** 2000, Micron-Resolution Velocimetry Techniques, *Developments in Laser Techniques and Application to Fluid Mechanics*, R.J. Adrian et al (Eds.), Springer-Verlag, Berlin
- Meinhart CD, Wereley ST, Gray MHB** 2000a, Depth effects in volume illuminated particle image velocimetry. *Meas. Sci. Technol.*, Vol. 11, p. 809-814
- Meinhart CD, Wereley ST, Santiago JG** 2000b, A PIV algorithm for estimating time-averaged velocity fields, *Journal of Fluids Engineering*, Vol. 122, 285-289
- Meinhart CD, Wereley ST, Santiago JG** 1999, PIV measurements of a microchannel flow, *Exp. Fluids*, Vol. 27, 414-419
- Meinhart CD and Zhang H** 2000, The flow structure inside a microfabricated inkjet printer head, *J. Microelectromechanical Systems*, Vol. 9, 67-75
- Modarress D, Fourquette D, Tuagwalder F, Gharib M, Forouhar S, Wilson D, Scalf J** 1998, Miniature and micro-Doppler sensors. *9<sup>th</sup> International Symposium on "Applications of Laser Techniques to fluid Mechanics"*, Lisbon, Portugal, July 13-16

- Modarress D, Fourquette D, Gharib M, Tuagwalder F, Forouhar S, Wilson D, Scalf J** 2000, Design and development of miniature and micro-Doppler sensors, *ASME FEDSM'2000, ASME 2000 Fluids Engineering Division Summer Meeting*, June 11-15, Boston, Massachusetts
- Northrup MA, Hills RF, Landre R, Lehew HD, Watson RA** 1995, A MEMS-based DNA analysis system, *Transducers'95, Eighth International Conference on Solid State Sensors and Actuators*, Stockholm, Sweden, June, pp. 764-767
- Olsen MG, Adrian RJ** 2001, Brownian motion and correlation in particle image velocimetry. Submitted to *Meas. Sci. Technol.*
- Paul PH, Garguilo MG, Rakestraw DJ** 1998, Imaging of pressure- and electrokinetically-driven flows through open capillaries. *Anal. Chem.* 70: 2459-2467
- Santiago JG, Wereley ST, Meinhart CD, Beebe DJ, Adrian RJ** 1998a, A particle image velocimetry system for microfluidics. *Exp. Fluids* 25, 316-319
- Takehara K, Adrian RJ, Etoh T** 1999, A hybrid correlation/Kalman filter/ $\chi^2$ -test method of super resolution PIV, *3<sup>th</sup> International Workshop on PIV'99 – Santa Barbara*, Sept. 16-18, Santa Barbara, CA
- Tieu AK, Mackenzie MR, Li EB** 1995, Measurements in microscopic flow with a solid-state LDA. *Exp. Fluids*, Vol. 19, pp. 293 – 294
- Wereley ST, Santiago JG, Meinhart CD, Adrian RJ** 1998, Velocimetry for MEMS Applications. *Proc. of ASME/DSC*, Vol. 66, (*Micro-fluidics Symposium*, Nov. 1998, Anaheim, CA)
- Wereley ST, Meinhart CD, Gray MHB** 1999, Depth effects in volume illuminated particle image velocimetry. *3<sup>th</sup> International Workshop on PIV'99 – Santa Barbara*, Sept. 16-18, Santa Barbara, CA
- Wereley ST, Meinhart CD** 2000a, Accuracy improvements in particle image velocimetry, *10<sup>th</sup> International Symposium on “Applications of Laser Techniques to fluid Mechanics”*, Lisbon, Portugal, July
- Wereley ST, Meinhart CD** 2000b, Adaptive second-order accurate particle image velocimetry, *Exp. Fluids* (in press)
- Wildes RP, Amable MJ Lanzilloto AM, Leu TS** 1997, Physically based fluid flow recovery from image sequences. *1997 IEEE*: 969-975